processes

MDPI

Article

Performance Analysis of a Calcium Looping Process Integrating Biomass Sorption-Enhanced Gasification with $CaCO_3$-Based Methane Reforming

Shuaijie Xue [1,*], Xudong Wang [2] and Guofu Liu [3]

[1] Science and Technology on Combustion, Internal Flow and Thermo-Structure Laboratory, Northwestern Polytechnical University, Xi'an 710072, China
[2] Jiangsu Key Laboratory of Process Enhancement & Energy Equipment Technology, School of Mechanical and Power Engineering, Nanjing Tech University, Nanjing 211816, China; xdwang_seu@seu.edu.cn
[3] School of Energy and Power Engineering, Qilu University of Technology (Shandong Academy of Sciences), Jinan 250353, China; golfliu@qlu.edu.cn
* Correspondence: xueshj@nwpu.edu.cn

Abstract: The growing demand for sustainable energy solutions has led to significant interest in biomass gasification and methane reforming. To address this demand, a novel calcium looping process (CaLP) is proposed, which integrates biomass sorption-enhanced gasification (BSEG) with in situ calcium $CaCO_3$-based methane reforming (CaMR). This process eliminates the need for $CaCO_3$ calcination and facilitates the in situ utilization of CO_2. The effects of gasification temperature, steam flowrate into the gasifier $\alpha_{G(H2O/C)}$, reforming temperature, and steam flowrate into the reformer $\alpha_{R(H2O/C)}$ were systematically evaluated. Increasing the gasification temperature from 600 °C to 700 °C enhances CO and H_2 yields from 0.653 to 11.699 kmol/h and from 43.999 to 48.536 kmol/h, respectively. However, CaO carbonation weakens, reducing CaO conversion from 79.15% to 48.38% and increasing CO_2 release. A higher $\alpha_{G(H2O/C)}$ promotes H_2 yield while suppressing CO and CH_4 formation. In the CaMR process, raising the temperature from 700 °C to 900 °C improves CH conversion from 64.78% to 81.29%, with a significant increase in CO and H_2 production. Furthermore, introducing steam into the reformer enhances H_2 production and CH_4 conversion, which reaches up to 97.30% at $\alpha_{R(H2O/C)}$ = 0.5. These findings provide valuable insights for optimizing integrated biomass gasification and methane reforming systems.

Keywords: biomass gasification; calcium looping process; closed-loop carbon utilization; methane reforming; thermodynamic modeling

check for updates

Academic Editor: Francesca Raganati

Received: 26 February 2025
Revised: 12 March 2025
Accepted: 17 March 2025
Published: 18 March 2025

Citation: Xue, S.; Wang, X.; Liu, G. Performance Analysis of a Calcium Looping Process Integrating Biomass Sorption-Enhanced Gasification with $CaCO_3$-Based Methane Reforming. *Processes* **2025**, *13*, 892. https://doi.org/10.3390/pr13030892

Copyright: © 2025 by the authors. Licensee MDPI, Basel, Switzerland. This article is an open access article distributed under the terms and conditions of the Creative Commons Attribution (CC BY) license (https://creativecommons.org/licenses/by/4.0/).

1. Introduction

The escalating global demand for clean and sustainable energy has catalyzed extensive research into alternative energy sources and sophisticated energy-conversion technologies. The efficient utilization of carbon-neutral fuels and carbon capture have both become important trends in the field of energy. Biomass, recognized as a renewable and carbon-neutral resource, has come to the fore as a promising alternative fuel [1,2].

Various methods exist for biomass utilization, among which gasification stands out as a compelling thermochemical conversion technique. This technology holds significant potential for the production of syngas, heat, renewable power, hydrogen, and chemicals [3–5], as it offers the potential to overcome the fluctuations in quality and calorific value of feedstocks. However, traditional biomass gasification faces challenges such as

low hydrogen yield, tar formation, and carbon dioxide emissions [6]. Additionally, the syngas is always diluted by nitrogen. To address these issues, the integration of biomass steam gasification with calcium looping processes (CaLP) has attracted attention due to its potential to enhance hydrogen production and enable efficient carbon dioxide capture, forming sorption-enhanced gasification (SEG) [7–10]. The hydrogen concentration in syngas from SEG is usually higher than 70% [7]. In SEG, the CO_2 capture capacity as well as the stability of the bed material have a huge influence on the performance of the SEG process. Previously, different CO_2 sorbents were employed to investigate the gasification performance, such as the CaO, MgO, and Li_4SiO_4. It was found that SEG with a CaO sorbent can produce syngas with the highest hydrogen concentration [11]. Consequently, CaO-based sorbents have been predominantly utilized as the bed material in the SEG process, primarily due to their superior CO_2 capture capacity and economic viability. This process is shown in Figure 1a. Both the feedstock and steam are fed into the gasifier while the CO_2 sorbent (typically CaO) circulates into it simultaneously. During the biomass steam gasification process, CaO reacts with CO_2 to shift the equilibrium of the reactions to improve the hydrogen yield. The carbonation product, $CaCO_3$, is then calcined in a calciner for CaO regeneration.

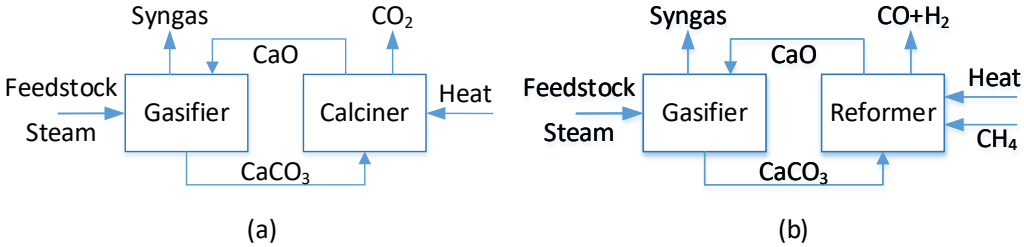


Figure 1. Principles of CaLP: (**a**) traditional CaLP; (**b**) SEG coupled with CaMR.

Different sorbents of limestones are employed in a lab-scale dual interconnected fluidized bed (DIFB) reactor for biomass SEG (BSEG) [12]. In an experimental demonstration using a 30 kW_{th} bubbling fluidized bed reactor, the SEG was tested with municipal solid waste as feedstock. The results reveal that the SEG exhibited a commendable performance in preventing tar formation, maintaining a content of as low as 7 g/Nm^3 [13]. In the same pilot plant, the SEG of sewage sludge was compared with steam–oxygen gasification, showing a high H_2 content of 70–73% [14]. Adjusting the steam-to-carbon ratio and the utilization of a high-sorption-capacity CO_2 sorbent are proven to be effective strategies for modifying the H/C ratio in syngas [15]. Mbeugang et al. conducted an experimental investigation into the SEG performance of cellulose within a fixed-bed reactor. Their findings suggest that the role of CaO as either a CO_2 absorbent or a catalyst is intrinsically linked to the gasification temperature [16]. In a bubbling fluidized reactor, the BSEG of sawdust was experimentally studied by Han et al. [17]. The highest concentration of hydrogen reached 62% and the optimal conditions were found at CaO/C = 1, H_2O/C = 2.18, and T = 740 °C.

In addition to experimental investigation, simulation provides a useful tool for system evaluation and optimization [18,19]. Pitkäoja et al. proposed a strategy for H_2O staging to tailor the gas composition of syngas derived from BSEG. Their research indicated that employing H_2O staging and cooling in a fluidized bed gasifier significantly boosted the carbonation of limestone and water–gas shift reactions [20]. A process simulation model for the SEG of corn stalk was established, in which the steam gasification and CO_2 sorption were separated in two stages to enhance the H_2 yield [21]. Although this increased the hydrogen yield, the reaction system was more complex. A modified thermodynamic equilibrium model was established for BSEG, which had high accuracy compared with the experimental results. Any increase in temperature, CaO/C, and steam/biomass helped to

increase the H_2 concentration in the syngas [22]. Santos et al. evaluated the techno-economic feasibility of the SEG, demonstrating a higher H_2 production efficiency when using SEG compared to traditional steam gasification [23]. In a techno-economic assessment by Cormos, green hydrogen generation from BSEG obtained good results, with high efficiency, a low energy cost, few economic penalties, and negative CO_2 emissions [24]. As the SEG showed a favorable performance for hydrogen generation and carbon capture, it was integrated with other systems, such as thermal energy storage [25].

Furthermore, the conversion of CH_4, another greenhouse gas, has attracted much attention. The dry reforming of methane (DRM) utilizes the CO_2, converting it into CO and H_2, and thereby reducing the greenhouse gases into fuels [26,27]. While CO_2 capture using CaO can form $CaCO_3$, a method of calcium looping coupled with DRM has already been proposed and widely studied in the field of post-combustion CO_2 capture [26,28–31]. Zhang et al. developed an integrated process of CaLP and in situ DRM using Fischer–Tropsch, which reduces the heat energy demand, with a drop of 28.08% [32]. This demonstrates the advances of integrating process CaLP with DRM.

It was shown that the BSEG is beneficial in generating high-quality syngas with adjustable gas compositions while $CaCO_3$ is formed. For the regeneration of CaO, this work proposes coupling it with DRM, instead of the traditional calcination. The principle of the proposed CaLP, integrating BSEG and $CaCO_3$-based methane reforming (CaMR), is shown in Figure 1b. In contrast to conventional CaLP, which relies on energy-intensive high-temperature calcination for CaO regeneration, this study proposes an innovative integration of BSEG with CaMR. The novelty lies in utilizing $CaCO_3$ (generated during BSEG) as a feedstock for methane reforming, thereby eliminating the need for calcination while enabling in situ CO_2 utilization. This dual-function approach simultaneously regenerates CaO for CO_2 capture and converts methane into syngas, enhancing process efficiency and reducing the carbon footprint. Prior studies primarily focused on standalone BSEG or methane reforming; this work bridges the two processes, establishing a synergistic pathway for sustainable energy production. The integration of BSEG and CaMR introduces a closed-loop carbon-utilization strategy.

The global demand for rice is projected to increase by over 1.2% annually, in response to the escalating food requirements caused by worldwide population growth and economic development [33]. Typically, the processing of one ton of rice results in the generation of approximately 240 kg of husks [34]. Consequently, the production of rice husks is a significant global phenomenon. Its valorization aligns with the principles of circular economy principles. Thus, rice husk was chosen as the feedstock in this work. To evaluate the performance of the proposed process, a thermodynamic process model was established based on the Gibbs free energy minimization to analyze the effects of different operating parameters on product distribution in both the gasifier and the reformer. The results demonstrate the feasibility of this CaLP and offer a practical concept for the conversion of methane.

2. Model of the Calcium Looping Process

Rice husk is a globally abundant agricultural residue, particularly in rice-producing regions. Utilizing it aligns with the circular economy principles as it valorizes waste. Due to its abundance, low cost, and carbon neutrality, it has been used as an alternative fuel in many fields. Therefore, rice husk was used as the feedstock for the BSEG. The proximate and ultimate analyses of the rice husk were derived from the literature and are presented in Table 1 [35].

Table 1. The proximate and ultimate analyses of the rice husk [35].

Item	Proximate Analysis				Ultimate Analysis				
	FC	Moisture	Volatiles	Ash	C	H	O	N	S
wt%	15.56	8.95	63.78	11.71	40.44	4.62	34.02	0.26	0

In this work, a thermodynamic analysis model is established to investigate the coupling cycle of BSEG and CaMR. As has been mentioned, CaO can play multiple roles in the biomass gasification process, namely as a catalyst for tar-cracking and as a CO_2 sorbent. It was used as the bed material for BSEG. The CaLP process integrating BSEG and CaMR is principally shown in Figure 2, and consists of a gasifier, reformer, and other components.

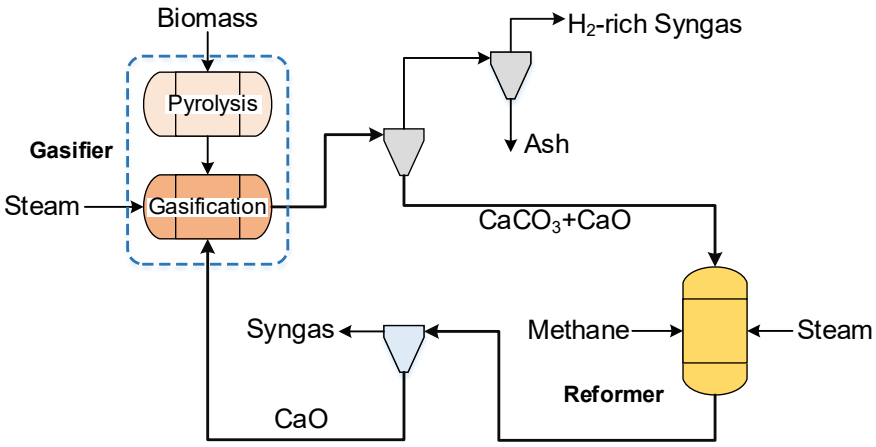


Figure 2. Principle process of the CaLP integrating BSEG with CaMR.

When the rice husk (RH) is fed into the gasifier, it goes through a fast pyrolysis step and the products are then gasified with the addition of the gasification agent. During the pyrolysis period, the volatiles are evaporated from the solid phase and some of them form tar. The reaction can be described as follows:

$$RH \rightarrow Char(C) + Tar + Gases(CO, H_2, H_2O, CH_4, C_2H_4, C_2H_6, CO_2) + Ash \quad (1)$$

Usually, the tar undergoes a second thermal decomposition period with the catalyst. As the CaO serves as the catalyst for tar-cracking, while the tar can be converted to syngas in the steam gasification period, the tar is regarded as having been totally converted into light hydrocarbons in this work.

The pyrolysis products then react with the gasification agent steam. The gasification period relates to many reactions and is quite complex. The gasification period should consist of the following reactions:

$$C + CO_2 \rightarrow 2CO \quad (2)$$

$$C + H_2O \rightarrow CO + H_2 \quad (3)$$

$$CO + H_2O \leftrightarrow CO_2 + H_2 \quad (4)$$

$$CO + 3H_2 \leftrightarrow CH_4 + H_2O \quad (5)$$

$$CO_2 + 4H_2 \leftrightarrow CH_4 + 2H_2O \quad (6)$$

$$CH_4 \leftrightarrow C + 2H_2 \quad (7)$$

$$CH_4 + CO_2 \leftrightarrow 2CO + 2H_2 \quad (8)$$

Additionally, the light hydrocarbons (e.g., C_2H_4 and C_2H_6) can also react with steam:

$$C_2H_4+2H_2O\leftrightarrow 2CO+4H_2 \quad (9)$$

$$C_2H_6+2H_2O\leftrightarrow 2CO+5H_2 \quad (10)$$

When the CaO is introduced into the gasifier, it can react with CO_2 and weaken the CO_2 partial pressure to shift the equilibria. The CaO carbonation is given as follows:

$$CaO+CO_2\rightarrow CaCO_3 \quad (11)$$

By shifting the equilibria, this reaction in gasifier is beneficial to enhance the purity of the H_2 in syngas and lowers the operating temperatures for RH gasification.

After BSEG, the solid phase is separated from the gaseous products in two separators. The $CaCO_3$ and unconverted CaO then flow into the reformer. Meanwhile, a stream of CH_4 is introduced into the reformer for the reforming reactions. In the reformer, the $CaCO_3$ can be decomposed into CaO and CO_2. The CO_2 can react with CH_4 for the dry reforming process. In addition, $CaCO_3$ may react with CH_4 directly for the in situ reforming. During this process, CaO is regenerated. After separation, the gaseous CaMR products are separated from the CaO. Then, the regenerated CaO is circulated into the gasifier for a whole CaLP integrating BSEG and CaMR.

3. Data Processing and Parameter Settings

3.1. Data Processing

In the CaLP process, the products of the reformer and gasifier are influenced by many operating parameters. Once the feeding rate of the RH is specific, the carbon content can be determined. In the gasifier, the CaO and the steam are introduced simultaneously with the RH. To evaluate the amount of steam, the equivalence ratio of steam to carbon in the gasifier $\alpha_{G(H2O/C)}$ is defined as follows:

$$\alpha_{G(H_2O/C)} = \frac{n_{G,steam}}{n_C} \quad (12)$$

where $n_{G,steam}$ is the molar flowrate of the steam flowing into the gasifier and the n_C is the molar flowrate of the carbon in the feedstock, which can be calculated according to the feeding rate of the RH and the ultimate analysis.

Correspondingly, the equivalence ratio of steam to carbon in the reformer $\alpha_{R(H2O/C)}$ is defined as follows:

$$\alpha_{R(H_2O/C)} = \frac{n_{R,steam}}{n_C} \quad (13)$$

where $n_{R,steam}$ is the molar flowrate of the steam flowing into the reformer.

In the gasifier, the CaO reacts with CO_2 to realize its conversion. The CaO conversion is the ratio of converted CaO ($CaCO_3$) to the total CaO into the gasifier, namely,

$$CaO \quad conversion=\frac{n_{CaCO_3}}{n_{CaO}+n_{CaCO_3}} \quad (14)$$

in which n_{CaO} and n_{CaCO3} are the molar flowrates of the CaO and $CaCO_3$ at the outlet of the gasifier, respectively.

In the reformer, the CH_4 is converted via reforming reactions. Its conversion is defined as the ratio of converted CH_4 to CH_4 in the reformer, which can be calculated by the following equation:

$$CH_4 \quad conversion=1-\frac{n_{CH_4,out}}{n_{CH_4,in}} \quad (15)$$

where $n_{CH_4,out}$ and $n_{CH_4,in}$ are the molar flowrates of the CH_4 flowing out of and into the reformer, respectively.

3.2. Parameter Settings

In the process simulation, the feeding rate of the RH is specified as 1000 kg/h. From the ultimate analysis results, the corresponding carbon flowrate is approximately 33.7 kmol/h. In these cases, the molar flowrate of the CaO into the gasifier is set to the same as that of the carbon. Additionally, the molar flowrate of the CH_4 into the reformer is set as 30 kmol/h. Under the fundamental condition, the temperature of the gasifier is 650 °C while that of the reformer is 800 °C. The $\alpha_{G(H2O/C)}$ and $\alpha_{R(H2O/C)}$ are set as 1 and 0, respectively. That means the dominant reaction in the reformer is the dry reforming of CH_4 under the fundamental condition.

For the established thermodynamic process model, the pyrolysis products in the gasifier are obtained based on the component yields, calculated using the mass balance of different elements. The gasification products and the reformer products are calculated based on the principle of Gibbs free energy minimization. Both the phase equilibrium and chemical equilibrium are realized by determining the composition of a system that minimizes the Gibbs free energy, subject to constraints, material balances, and the specified temperature and pressure.

4. Performance of CaLP Integrating BSEG with CaMR

4.1. Effects of the Gasification Temperature

When the gasification temperature increased from 600 °C to 700 °C, the other parameters remained constant with those under the fundamental conditions. The products at the outlet of the gasifier are shown in Figure 3.

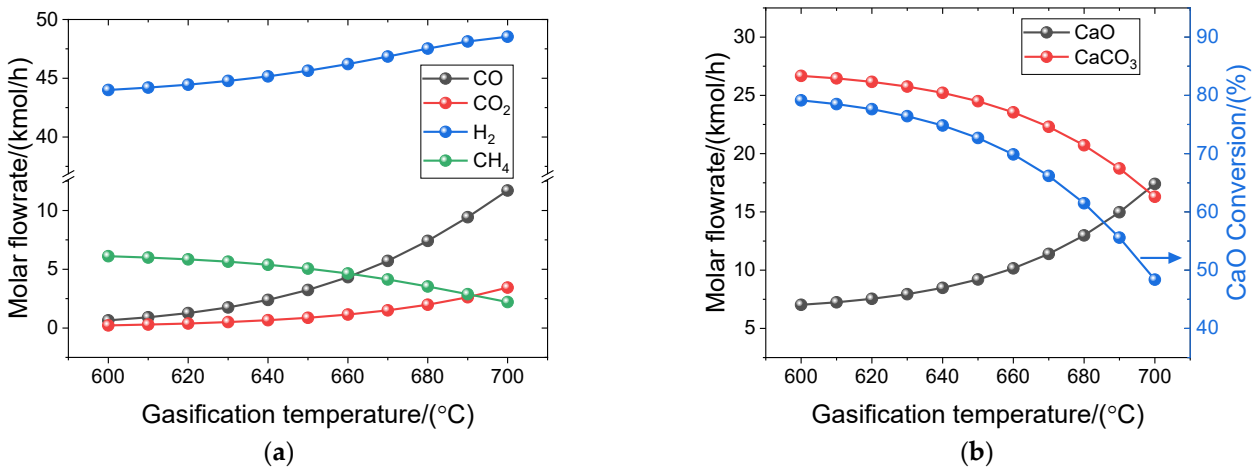


Figure 3. Effects of the gasification temperature on the BSEG products: (**a**) gaseous products; (**b**) solid products and CaO conversion.

It is shown that when the gasification temperature increased from 600 °C to 700 °C, the flowrates of CO and CO_2 exhibited an increasing trend. Specifically, the CO at the outlet of the gasifier increased from 0.653 kmol/h at 600 °C to 11.699 kmol/h at 700 °C, while the CO_2 increased from 0.220 kmol/h to 3.440 kmol/h over the same temperature range. This indicates enhanced carbon monoxide and carbon dioxide production at higher temperatures. The increase in CO and CO_2 can be attributed to the endothermic nature of gasification reactions, such as the Boudouard reaction and char steam gasification, which are enhanced at elevated temperatures [36,37]. Additionally, the calcium oxide serves as a CO_2 sorbent. When the temperature increases, the carbonation reaction of CaO is

weakened, which leads to an increased generation of CO_2. A higher CO_2 content can promote the char CO_2 gasification and CH_4 reforming reactions in the reaction system. Meanwhile, the H_2 in syngas showed a gradual increase, from 43.999 kmol/h at 600 °C to 48.536 kmol/h at 700 °C, suggesting a relatively stable but slightly improved hydrogen yield. This increase is likely due to the enhanced steam gasification and water–gas shift reactions that occur at higher temperatures, which are facilitated by the presence of CaO. The molar ratio of H_2/CO in syngas decreased from 67.38 to 4.15. The sorption of CO_2 by CaO shifts the equilibrium of these reactions toward H_2 production, contributing to the increase in hydrogen generation. However, from the perspective of the volume concentration, the H_2 concentration in the dry-basis syngas decreased from 86.15% to 73.56% as the temperature increased. However, the CH_4 flowrate declined from 6.108 kmol/h to 2.212 kmol/h when the temperature increased from 600 °C to 700 °C. This decrease can be explained by the endothermic methane reforming reactions, which become more dominant at higher temperatures, leading to the decomposition of methane into CO and H_2. This is in close alignment with the reforming property of CH_4 [38]. Additionally, the CaO may react with the CO_2 during the BSEG process, suppressing CH_4 formation. These trends highlight the temperature-dependent behavior of the BSEG process, with higher temperatures favoring the production of CO and H_2. The role of CaO as a CO_2 sorbent can enhance the gasification process and dramatically improve the overall hydrogen yield by shifting the reaction equilibria.

As for the solid-phase products, the CaO at the gasifier outlet increased steadily, from 7.027 kmol/h at 600 °C to 17.397 kmol/h at 700 °C, while the $CaCO_3$ decreased from 26.673 kmol/h to 16.303 kmol/h during the BSEG process. The carbonation reaction between CaO and CO_2 is exothermic and increasing the temperature shifts the equilibrium toward the reactants, reducing the formation of $CaCO_3$. During this process, the CaO conversion correspondingly decreased from 79.15% to 48.38%. This decrease in CaO conversion at higher temperatures aligns with the increase in CO_2 flowrates in the gasification products. As CaO captures less CO_2, more CO_2 is released into the gas stream and shifts the equilibrium of the gasification reactions toward CO formation. Though high temperatures are beneficial to gasification, they weaken the sorption reaction between CaO and CO_2, which negatively impacts the CO_2 capture and the generation of hydrogen-rich syngas.

The effects of the gasification temperature on the CaMR products are shown in Figure 4.

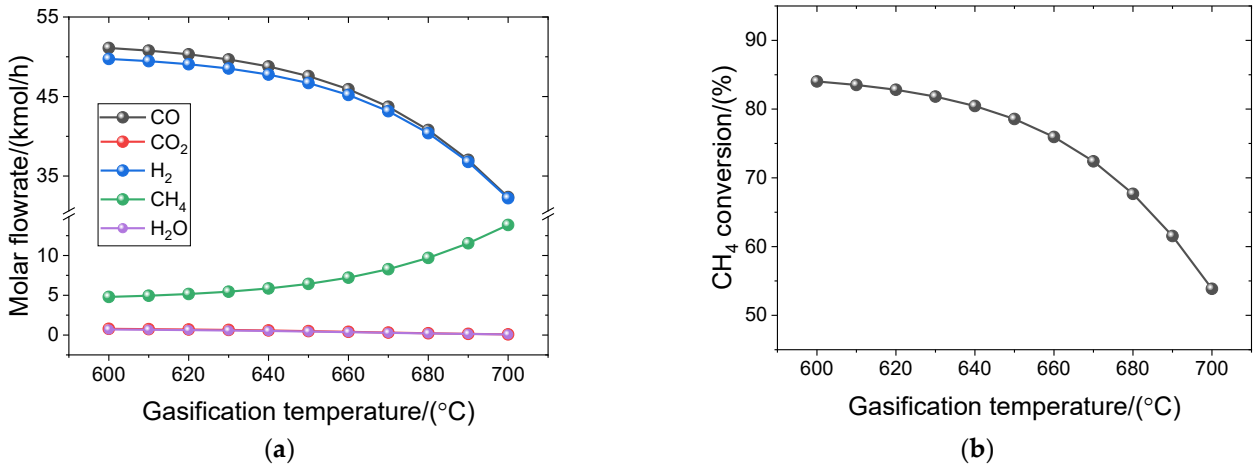


Figure 4. Effects of the gasification temperature on the CaMR products: (**a**) gaseous products; (**b**) CH_4 conversion.

When the gasification temperatures changed, the $CaCO_3$ flowing into the downstream reformer varied from 26.673 kmol/h to 16.303 kmol/h and showed the ability to react with

methane for reforming. When the gasification temperature increased from 600 °C to 700 °C, the flowrate of CO decreased from 51.103 kmol/h to 32.361 kmol/h, while H_2 decreased from 49.724 kmol/h to 32.222 kmol/h. This indicates that a higher $CaCO_3$ flowrate can increase CO and H_2 production in the reforming process. During this process, the CO_2 flowrate decreased from 0.777 kmol/h to 0.084 kmol/h as the gasification temperature increased. Similarly, the H_2O flow rate decreased from 0.690 kmol/h to 0.076 kmol/h. This suggests that a higher $CaCO_3$ flowrate results in more CO_2 and H_2O being produced from the $CaCO_3$ decomposition and/or the CH_4 reforming. Under the simulated conditions, the model predicts negligible carbon formation due to the suppression of methane cracking and the Boudouard reaction. Additionally, as seen in the calculation results, due to some side reactions, H_2O is produced. The absence of steam in the methane reforming system is beneficial to avoid the decomposition of the coke. However, the CH_4 flowrate at the reformer outlet increased from 4.792 kmol/h to 13.842 kmol/h, corresponding to a decrease in CH4 conversion in CaMR from 84.03% to 53.86%, as illustrated in Figure 4b.

During the CaMR process, the $CaCO_3$ may decompose at high temperatures to form CaO and CO_2. The produced CO_2 can then participate in the dry reforming of methane, which increases the production of CO and H_2. Thus, the CO and H_2 flowrate are positively related to the $CaCO_3$ flowing into the reformer. As the H_2O is generated, there must be some side reactions taking place in the reformer. It is clear that low flowrates of C_2H_4 and C_2H_6 are also produced in the reformer due to the side reactions, varying in from 0.390 mol/h to 5.691 mol/h and from 0.153 mol/h to 1.967 mol/h, respectively.

4.2. Effects of the Steam Flowrate into Gasifier

In the gasifier, the steam is an important gasification agent for the conversion of the rice husk. As has been mentioned in the previous section, the steam is involved in several relevant reactions in the BSEG process. When the equivalence steam-to-carbon ratio in the gasifier $\alpha_{G(H2O/C)}$ varies from 0.8 to 1.5, the products of BSEG are shown in Figure 5.

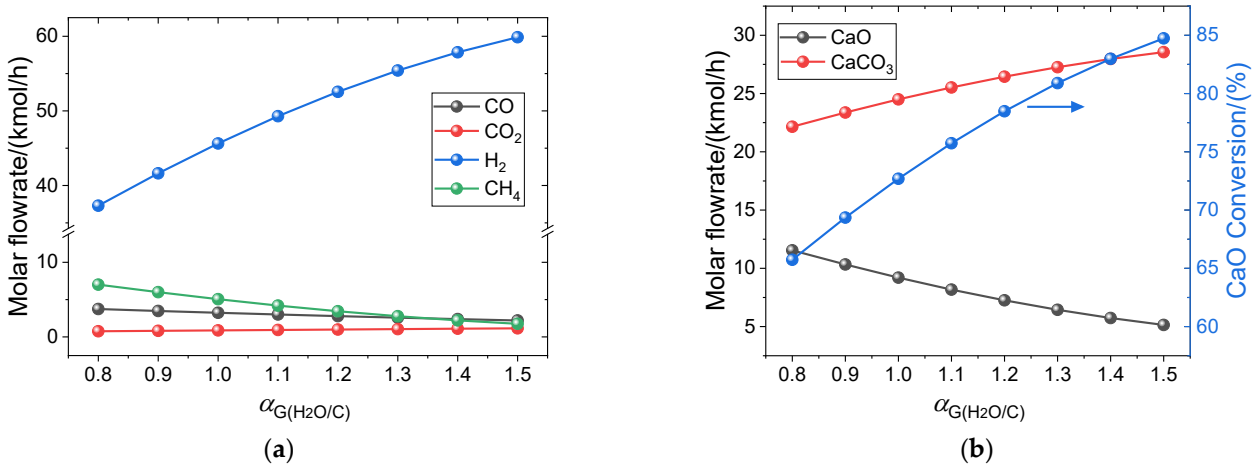


Figure 5. Effects of the $\alpha_{G(H2O/C)}$ on the BSEG products: (**a**) gaseous products; (**b**) solid products and CaO conversion.

As the equivalence ratio $\alpha_{G(H2O/C)}$ increased from 0.8 to 1.5, the flowrates of CO and CH_4 decreased at the outlet of the gasifier. In these cases, the CO flowrate dropped from 3.736 kmol/h to 2.197 kmol/h while that of CH_4 declined from 7.011 kmol/h to 1.752 kmol/h. In contrast, the flowrate of H_2 dramatically increased from 37.305 kmol/h to 59.879 kmol/h, which correspond to the increase in H_2 concentration from 76.29% to 92.02% (in dry basis). Meanwhile, the CO_2 flowrate slightly increased from 0.753 kmol/h to 1.151 kmol/h. These trends indicate that an increase in steam availability suppresses CO

and CH_4 formation while significantly promoting H_2 production. Additionally, the gradual increase in CO_2 and the sharp rise in H_2 suggest a shift in the dominant reaction pathways as the $\alpha_{G(H2O/C)}$ increases. These phenomena can be explained by the interplay of several key gasification reactions, which are influenced by the equivalence ratio $\alpha_{G(H2O/C)}$ and the presence of CaO. At a lower $\alpha_{G(H2O/C)}$, the primary reactions include the water–gas reaction and methane reforming reactions (dry reforming and/or steam reforming), which produce a large amount of H_2. These reactions are further enhanced by the presence of CaO, which captures CO_2 through the carbonation reaction, shifting the equilibrium of the water–gas shift and steam reforming reactions toward H_2 production. The decrease in CH_4 flowrate is a direct result of this enhanced reforming process. On the other hand, excess steam drives the water–gas shift reaction, converting CO into CO_2 and further increasing H_2 production. This explains the decline in CO and the rise in CO_2 and H_2 at a higher $\alpha_{G(H2O/C)}$. The steam in the gasifier has the dual roles of promoting both H_2 production and CO_2 generation, as well as showing the limitations of CaO in fully mitigating CO_2 release under high-steam conditions. These insights highlight the need to optimize this ratio to maximize H_2 production and minimize undesirable byproducts in the BSEG process.

When the $\alpha_{G(H2O/C)}$ increased from 0.8 to 1.5, the flowrate of CaO at the gasifier outlet gradually decreased from 11.547 kmol/h to 5.146 kmol/h, while that of $CaCO_3$ increased from 22.153 kmol/h to 28.554 kmol/h. This indicates that CaO is continuously consumed and converted into $CaCO_3$ during the BSEG process when more steam is introduced into the gasifier. Correspondingly, the CaO conversion rate increased from 65.74% to 84.73%. The presence of more steam in the gasifier can significantly affect CaO conversion via enhancing the reactions through CO_2 generation.

The effects of the equivalence ratio $\alpha_{G(H2O/C)}$ on the CaMR products are shown in Figure 6.

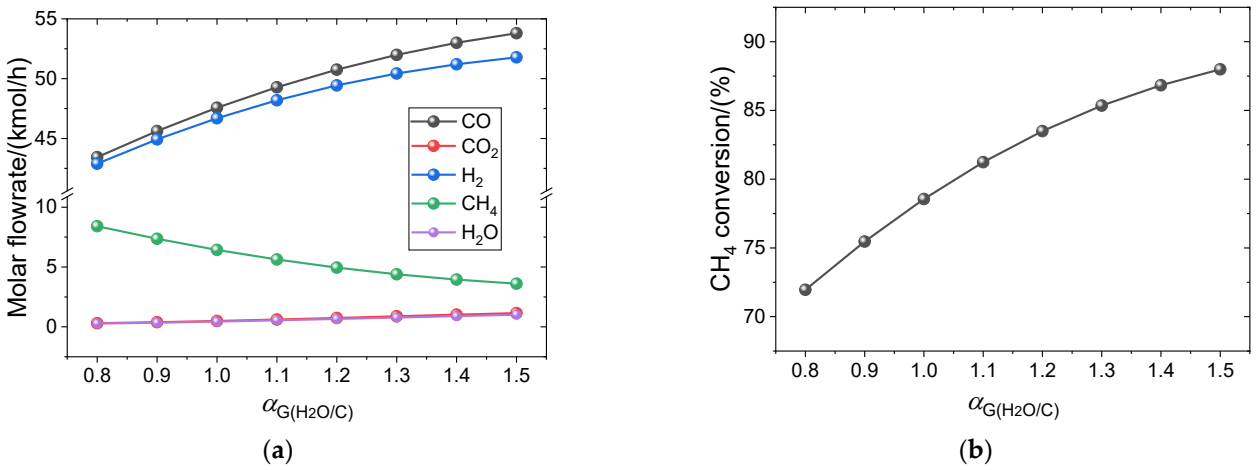


Figure 6. Effects of the $\alpha_{G(H2O/C)}$ on the CaMR products: (**a**) gaseous products; (**b**) CH_4 conversion.

When the equivalence ratio $\alpha_{G(H2O/C)}$ varied from 0.8 to 1.5, different $CaCO_3$ flowrates were introduced into the reformer. The flowrates of CO, CO_2, H_2, and H_2O at the reformer outlet showed a consistent upward trend. Specifically, the CO flowrate increased from 43.435 kmol/h to 53.802 kmol/h and the H_2 flowrate increased from 42.898 kmol/h to 51.785 kmol/h. The flowrates of CO_2 and H_2O have approximately the same variation trends. Specifically, when the $\alpha_{G(H2O/C)}$ increased from 0.8 to 1.5, the CO_2 flowrate rises from 0.300 kmol/h to 1.149 kmol/h, and H_2O increased from 0.271 kmol/h to 1.009 kmol/h. However, the CH_4 flowrate decreased significantly from 8.414 kmol/h to 3.603 kmol/h, indicating higher CH_4 consumption at a higher $\alpha_{G(H2O/C)}$. In the CaMR, $CaCO_3$ may decompose at high temperatures to produce CaO and CO_2. The CO_2 participates released

during the dry reforming of methane drive the production of CO and H_2. As the increase in $\alpha_{G(H2O/C)}$ results in an increase in the $CaCO_3$ flowrate into the reformer, more CO_2 is available for the dry reforming reaction, leading to higher CO and H_2 production and greater CH_4 consumption. Under these conditions, no steam is introduced into the reformer; however, steam is generated at the outlet. The reverse water–gas shift reaction may also contribute to the observed trends, as it further converts CO_2 and H_2 into CO and H_2O, particularly at higher $CaCO_3$ flowrates, due to the higher partial pressure of CO_2 in the reaction system. This can be demonstrated by the phenomenon that the increasing rate of CO is higher than that of H_2 at a higher $\alpha_{G(H2O/C)}$. As a comprehensive result, the CH_4 conversion in the reformer also increased in line with the $\alpha_{G(H2O/C)}$. When the $\alpha_{G(H2O/C)}$ increased from 0.8 to 1.5, the CH_4 conversion increased from 71.95% to 87.99%.

4.3. Effects of the Reforming Temperature

Under fundamental conditions, the CaO and $CaCO_3$ flowrates at the gasifier outlet were approximately 9.204 kmol/h and 24.496 kmol/h, respectively. They separated from syngas and flowed into the gasifier downstream. When the temperature of the reformer changed from 700 °C to 900 °C, the CaMR products obtained were as shown in Figure 7.

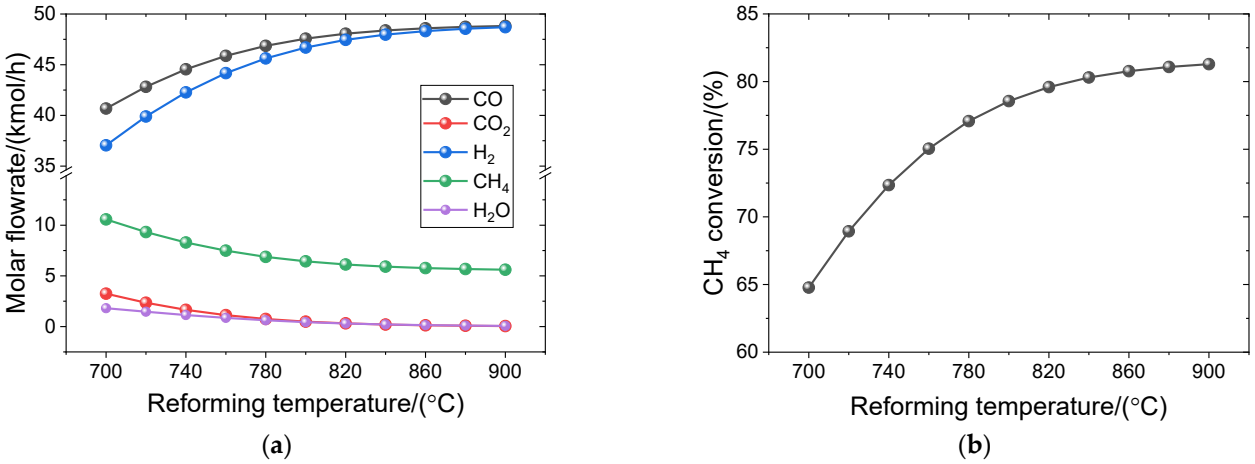


Figure 7. Effects of the reforming temperature on the CaMR products: (**a**) gaseous products; (**b**) CH_4 conversion.

The results illustrate the effects of reforming temperature variations on the product distribution in the CaMR process. As the temperature increased from 700 °C to 900 °C, the flowrate of CO increased from 40.68 kmol/h at 700 °C to 48.82 kmol/h at 900 °C. This increase is consistent with the endothermic nature of the reforming reactions, which favor higher temperatures. As another product of the reforming reaction, the flowrate of H_2 increased from 37.05 kmol/h at 700 °C to 48.70 kmol/h at 900 °C. This increase is consistent with the enhanced reforming reactions at higher temperatures, as mentioned previously. The flowrate of CO_2 decreased from 3.25 kmol/h at 700 °C to 0.052 kmol/h at 900 °C. Additionally, the decomposition of $CaCO_3$ releases CO_2, but this is rapidly consumed in the reforming process. The flowrate of CH_4 decreased from 10.57 kmol/h at 700 °C to 5.61 kmol/h at 900 °C, indicating an increase in CH_4 conversion at higher temperatures. This reduction is due to the consumption of CO_2 and CH_4 in the reforming reactions, particularly the dry reforming of CH_4, which becomes more favorable at higher temperatures. The generation of H_2O should be caused by side reactions such as the reverse water–gas shift reaction. Its flowrate decreased from 1.81 kmol/h at 700 °C to 0.066 kmol/h at 900 °C. This reduction is due to the consumption of H_2O in the steam reforming reaction and the water–gas shift reaction. The increase in CO and H_2 production,

along with the decrease in CH_4, CO_2, and H_2O, indicates that the reforming reactions favor higher temperatures, leading to more CH_4 being converted into syngas in CaMR. Interestingly, the side reactions can produce C_2H_4 and C_2H_6, as mentioned in the previous section. However, they show different variation trends. The flowrate of C_2H_4 increased from 0.244 mol/h to 4.312 mol/h with the increase in reforming temperature. The flowrate of C_2H_6 first decreased from 0.427 mol/h at 700 °C to 0.293 mol/h at 780 °C, then increased to 0.435 mol/h at 900 °C. Overall, the CH_4 conversion in CaMR increased from 64.78% to 81.29% as the temperature increased from 700 °C to 900 °C.

4.4. Effects of the Steam Flowrate into Reformer

It has been demonstrated that some side reactions in the reformer can produce H_2O. In reality, the addition of H_2O in the CH_4 reforming system is beneficial to avoid carbon deposition, changing it to a bio-reforming process. Therefore, a stream of steam was added to the reformer to investigate the effects of the steam flowrate on the CaMR process. The CaMR products obtained whenthe equivalence ratio $\alpha_{R(H2O/C)}$ increased from 0 to 0.5 are shown in Figure 8.

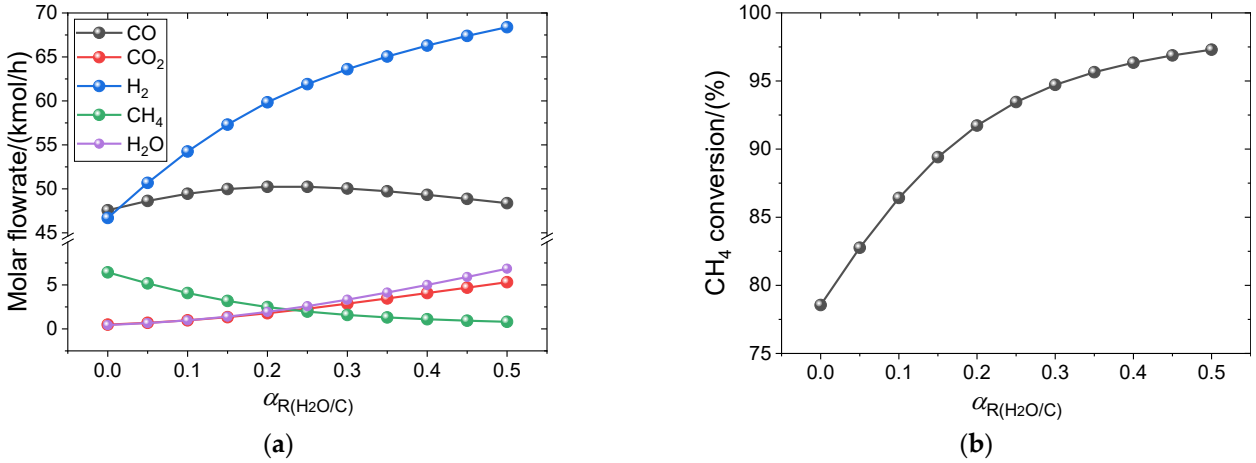


Figure 8. Effects of the $\alpha_{R(H2O/C)}$ on the CaMR products: (**a**) gaseous products; (**b**) CH_4 conversion.

As illustrated in Figure 8, the flowrate of CO initially increased from 47.57 kmol/h at $\alpha_{R(H2O/C)}$ = 0 to a maximum of 50.23 kmol/h at $\alpha_{R(H2O/C)}$ = 0.2, after which it gradually decreased to 48.38 kmol/h when the $\alpha_{R(H2O/C)}$ reached 0.5. This trend is caused by the competing effects of steam reforming and the water–gas shift reaction. At low steam flowrates, steam reforming dominates, leading to an increase in CO production. However, as steam flow increases further, the water–gas shift reaction becomes more significant, consuming CO and producing CO_2. The steam reforming reaction produces H_2 as a primary product while the water–gas shift reaction also contributes to H_2 production. As they are enhanced, hydrogen generation is improved. It is shown that the flowrate of H_2 increased substantially from 46.69 kmol/h to 68.38 kmol/h when the $\alpha_{R(H2O/C)}$ rises from 0 to 0.5. The flowrate of CO_2 increased steadily from 0.49 kmol/h at $\alpha_{R(H2O/C)}$ = 0 to 5.31 kmol/h at $\alpha_{R(H2O/C)}$ = 0.5. This increase is due to the water–gas shift reaction, which converts CO and H_2O into CO_2 and H_2. It may also be affected by the competing reactions of steam reforming and CO_2 reforming. When the steam flowrate increases, CO_2 reforming should be weakened due to the increase in the partial pressure of steam. When the $\alpha_{R(H2O/C)}$ increased from 0 to 0.5, the flowrate of H_2O at the outlet increases from 0.44 kmol/h to 6.85 kmol/h. However, the rate of the H_2O increase in the outlet is lower than the rate of the increase in inlet steam, indicating that more H_2O is consumed during the reactions. This is consistent with the increased activity observed in both steam

reforming and the water–gas shift reaction at higher steam flowrates. Correspondingly, the flowrate of CH_4 decreased from 6.43 kmol/h to 0.81 kmol/h as $\alpha_{R(H2O/C)}$ increased from 0 to 0.5, indicating improved CH_4 conversion with higher steam flowrates. This is expected because steam reforming is enhanced with an increase in steam availability, leading to the greater consumption of CH_4. In these cases, the generation of C_2H_4 and C_2H_6 is very low compared with that observed previously. As the methane reforming is enhanced, the CH_4 conversion increases from 78.56% to 97.30% in line with the increase in $\alpha_{R(H2O/C)}$.

The proposed integrated calcium looping process directly contributes to green hydrogen production by coupling biomass gasification with methane reforming. The integration of BSEG and CaMR eliminates energy-intensive calcination, enabling in situ CO_2 utilization and closed-loop carbon management. The SEG has a comparable economic feasibility with that of conventional steam gasification. If the cost of carbon capture is considered, SEG has significant advantages. While the CaMR is coupled, it reduces the CO_2 cost of methane reforming. For a detailed analysis of the techno-economic feasibility, further systemic work should be conducted.

5. Conclusions

This study presents a favorable integration of BSEG with CaMR within a novel CaLP. By replacing energy-intensive calcination with in situ CO_2 utilization, the system achieves closed-loop carbon management while maximizing hydrogen-rich syngas production. The key findings are summarized as follows:

(1) Increasing the gasification temperature in BSEG enhances CO production and H_2 yield, which are driven by endothermic reactions. However, higher temperatures reduce CaO conversion, leading to a lower CH_4 conversion in the downstream reformer.

(2) Increasing $\alpha_{G(H2O/C)}$ from 0.8 to 1.5 substantially improves H_2 production from 37.305 kmol/h to 59.879 kmol/h and increases CH_4 conversion from 71.95% to 87.99% in the reformer.

(3) Increasing the reforming temperature from 700 °C to 900 °C increases CH_4 conversion from 64.78% to 81.29%, indicating the more efficient utilization of CO_2 in reforming reactions at higher temperatures. Meanwhile, as $\alpha_{R(H2O/C)}$ rises from 0 to 0.5, CH_4 conversion improves dramatically from 78.56% to 97.30% while the H_2 flowrate in the reformer increases from 46.69 kmol/h to 68.38 kmol/h.

This technology bridges biomass utilization, carbon capture, and methane conversion. Future work should focus on experimental validation and techno-economic feasibility assessments.

Author Contributions: Conceptualization, S.X. and X.W.; methodology, S.X.; validation, X.W. and G.L.; formal analysis, S.X.; investigation, S.X. and G.L.; data curation, S.X.; writing—original draft preparation, S.X.; writing—review and editing, X.W. and G.L.; supervision, X.W.; funding acquisition, X.W. All authors have read and agreed to the published version of the manuscript.

Funding: This research was funded by the Natural Science Foundation of Jiangsu Province (BK20240547), Science and Technology Support Program of Jiangsu Province (BA2022103) and China Postdoctoral Science Foundation (2023M743917).

Data Availability Statement: The data are contained within the article.

Conflicts of Interest: The authors declare no conflicts of interest.

References

1. Awasthi, M.K.; Sar, T.; Gowd, S.C.; Rajendran, K.; Kumar, V.; Sarsaiya, S.; Li, Y.; Sindhu, R.; Binod, P.; Zhang, Z.; et al. A comprehensive review on thermochemical, and biochemical conversion methods of lignocellulosic biomass into valuable end product. *Fuel* **2023**, *342*, 127790. [CrossRef]
2. Wang, Y.; Wu, J.J. Thermochemical conversion of biomass: Potential future prospects. *Renew. Sustain. Energy Rev.* **2023**, *187*, 113754. [CrossRef]
3. Zhang, Y.; Wan, L.; Guan, J.; Xiong, Q.A.; Zhang, S.; Jin, X. A Review on Biomass Gasification: Effect of Main Parameters on Char Generation and Reaction. *Energy Fuels* **2020**, *34*, 13438–13455. [CrossRef]
4. Dai, J.; Whitty, K.J. Chemical looping gasification and sorption enhanced gasification of biomass: A perspective. *Chem. Eng. Process.* **2022**, *174*, 108902. [CrossRef]
5. Xu, D.; Yang, L.; Ding, K.; Zhang, Y.; Gao, W.; Huang, Y.; Sun, H.; Hu, X.; Syed-Hassan, S.S.A.; Zhang, S.; et al. Mini-Review on Char Catalysts for Tar Reforming during Biomass Gasification: The Importance of Char Structure. *Energy Fuels* **2020**, *34*, 1219–1229. [CrossRef]
6. Li, L.; Sun, G.; Wang, X.; Shao, Y. Thermodynamic analysis on the coupling effects of operating parameters in sorption-enhanced chemical looping gasification with rice husk as feedstock. *Int. J. Hydrogen Energy* **2024**, *85*, 346–359. [CrossRef]
7. Parvez, A.M.; Hafner, S.; Hornberger, M.; Schmid, M.; Scheffknecht, G. Sorption enhanced gasification (SEG) of biomass for tailored syngas production with in-situ CO_2 capture: Current status, process scale-up experiences and outlook. *Renew. Sustain. Energy Rev.* **2021**, *141*, 110756. [CrossRef]
8. Martínez, I.; Callén, M.S.; Grasa, G.; López, J.M.; Murillo, R. Sorption-enhanced gasification (SEG) of agroforestry residues: Influence of feedstock and main operating variables on product gas quality. *Fuel Process. Technol.* **2022**, *226*, 107074. [CrossRef]
9. Wang, Y.; Li, Y. Sorption-enhanced steam gasification of biomass for H2-rich gas production and in-situ CO_2 capture by CaO-based sorbents: A critical review. *Appl. Energy Combust. Sci.* **2023**, *14*, 100124. [CrossRef]
10. Martínez, I.; Romano, M.C. Flexible sorption enhanced gasification (SEG) of biomass for the production of synthetic natural gas (SNG) and liquid biofuels: Process assessment of stand-alone and power-to-gas plant schemes for SNG production. *Energy* **2016**, *113*, 615–630. [CrossRef]
11. Sikarwar, V.S.; Peela, N.R.; Vuppaladadiyam, A.K.; Ferreira, N.L.; Mašláni, A.; Tomar, R.; Pohořelý, M.; Meers, E.; Jeremiáš, M. Thermal plasma gasification of organic waste stream coupled with CO_2-sorption enhanced reforming employing different sorbents for enhanced hydrogen production. *RSC Adv.* **2022**, *12*, 6122–6132. [CrossRef]
12. Coppola, A.; Massa, F.; Montagnaro, F.; Scala, F. Analysis of the behaviour of limestone sorbents for sorption-enhanced gasification in dual interconnected fluidised bed reactor. *Fuel* **2023**, *340*, 127594. [CrossRef]
13. Martínez, I.; Grasa, G.; Callén, M.S.; López, J.M.; Murillo, R. Optimised production of tailored syngas from municipal solid waste (MSW) by sorption-enhanced gasification. *Chem. Eng. J.* **2020**, *401*, 126067. [CrossRef]
14. Moles, S.; Martinez, I.; Callén, M.S.; Gómez, J.; López, J.M.; Murillo, R. Pilot-scale study of sorption-enhanced gasification of sewage sludge. *Fuel* **2024**, *360*, 130611. [CrossRef]
15. Martínez, I.; Kulakova, V.; Grasa, G.; Murillo, R. Experimental investigation on sorption enhanced gasification (SEG) of biomass in a fluidized bed reactor for producing a tailored syngas. *Fuel* **2020**, *259*, 116252. [CrossRef]
16. Mbeugang, C.F.M.; Li, B.; Lin, D.; Xie, X.; Wang, S.; Wang, S.; Zhang, S.; Huang, Y.; Liu, D.; Wang, Q. Hydrogen rich syngas production from sorption enhanced gasification of cellulose in the presence of calcium oxide. *Energy* **2021**, *228*, 120659. [CrossRef]
17. Han, L.; Wang, Q.; Yang, Y.; Yu, C.; Fang, M.; Luo, Z. Hydrogen production via CaO sorption enhanced anaerobic gasification of sawdust in a bubbling fluidized bed. *Int. J. Hydrogen Energy* **2011**, *36*, 4820–4829. [CrossRef]
18. Wang, X.; Wang, R.; Shao, Y.; Jin, B. Performance evaluation on the chemical looping combustion of the chromium-containing leather waste and the fate of chromium using thermodynamic analysis. *Energy* **2025**, *315*, 133810. [CrossRef]
19. Xue, S.; Wang, X. Process simulation of chemical looping gasification of biomass using Fe-based oxygen carrier: Effect of coupled parameters. *J. Clean. Prod.* **2022**, *356*, 131839. [CrossRef]
20. Pitkäoja, A.; Ritvanen, J. Simulation of sorption-enhanced gasification: H_2O staging to a circulating fluidised bed gasifier to tailor the producer gas composition. *Energy* **2023**, *266*, 126446. [CrossRef]
21. Li, B.; Mbeugang, C.F.M.; Liu, D.; Zhang, S.; Wang, S.; Wang, Q.; Xu, Z.; Hu, X. Simulation of sorption enhanced staged gasification of biomass for hydrogen production in the presence of calcium oxide. *Int. J. Hydrogen Energy* **2020**, *45*, 26855–26864. [CrossRef]
22. Li, C.; Liu, R.; Zheng, J.; Zhang, Y. Thermodynamic study on the effects of operating parameters on CaO-based sorption enhanced steam gasification of biomass. *Energy* **2023**, *273*, 127208. [CrossRef]
23. Santos, M.P.S.; Hanak, D.P. Techno-economic feasibility assessment of sorption enhanced gasification of municipal solid waste for hydrogen production. *Int. J. Hydrogen Energy* **2022**, *47*, 6586–6604. [CrossRef]
24. Cormos, C. Decarbonized green hydrogen production by sorption-enhanced biomass gasification: An integrated techno-economic and environmental evaluation. *Int. J. Hydrogen Energy* **2024**, *95*, 592–603. [CrossRef]

25. Khosravi, S.; Neshat, E.; Saray, R.K. Thermodynamic analysis of a sorption-enhanced gasification process of municipal solid waste, integrated with concentrated solar power and thermal energy storage systems for co-generation of power and hydrogen. *Renew. Energy* **2023**, *214*, 140–153. [CrossRef]
26. Papalas, T.; Antzaras, A.N.; Lemonidou, A.A. Integrated CO_2 Capture and Utilization by Combining Calcium Looping with CH_4 Reforming Processes: A Thermodynamic and Exergetic Approach. *Energy Fuels* **2024**, *38*, 11966–11979. [CrossRef]
27. Li, J.; He, X.; Hu, R. Integrated Carbon Dioxide Capture and Utilization for the Production of CH_4, Syngas and Olefins over Dual-Function Materials. *Chemcatchem* **2024**, *16*, e202301714. [CrossRef]
28. Tian, S.; Yan, F.; Zhang, Z.; Jiang, J. Calcium-looping reforming of methane realizes in situ CO_2 utilization with improved energy efficiency. *Sci. Adv.* **2019**, *5*, eaav5077. [CrossRef]
29. Sun, S.; Zhang, C.; Wang, Y.; Zhao, X.; Sun, H.; Wu, C. CO_2 capture from H_2O and O_2 containing flue gas integrating with dry reforming methane using Ni-doping CaO dual functional materials. *Chem. Eng. J.* **2023**, *468*, 143712. [CrossRef]
30. Hu, J.; Hongmanorom, P.; Chirawatkul, P.; Kawi, S. Efficient integration of CO_2 capture and conversion over a Ni supported CeO_2-modified CaO microsphere at moderate temperature. *Chem. Eng. J.* **2021**, *426*, 130864. [CrossRef]
31. Jo, S.; Gilliard-AbdulAziz, K.L. Self-Regenerative Ni-Doped $CaTiO_3$/CaO for Integrated CO_2 Capture and Dry Reforming of Methane. *Small* **2024**, *20*, e2401156. [CrossRef] [PubMed]
32. Zhang, C.; Li, Y.; Chu, Z.; Fang, Y.; Han, K.; He, Z. Analysis of integrated CO_2 capture and utilization via calcium-looping in-situ dry reforming of methane and Fischer-Tropsch for synthetic fuels production. *Sep. Purif. Technol.* **2024**, *329*, 125109. [CrossRef]
33. Mishra, A.; Taing, K.; Hall, M.W.; Shinogi, Y. Effects of rice husk and rice husk charcoal on soil physicochemical properties, rice growth and yield. *Agric. Sci.* **2017**, *8*, 1014–1032. [CrossRef]
34. Okeh, O.C.; Onwosi, C.O.; Odibo, F.J.C. Biogas production from rice husks generated from various rice mills in Ebonyi State, Nigeria. *Renew. Energy* **2014**, *62*, 204–208. [CrossRef]
35. Cheng, S.; Jin, B.; Wang, L.; Cao, S.; He, T.; Chen, Y.; Su, X.; Gu, Q.; Zhang, W.; Sheng, P.; et al. Design and operation of a demonstration plant for fluidized bed low-temperature gasification of alternative fuels applied to cement production. *Chem. Eng. J.* **2024**, *502*, 158117. [CrossRef]
36. Lahijani, P.; Zainal, Z.A.; Mohammadi, M.; Mohamed, A.R. Conversion of the greenhouse gas CO_2 to the fuel gas CO via the Boudouard reaction: A review. *Renew. Sustain. Energy Rev.* **2015**, *41*, 615–632. [CrossRef]
37. Prestipino, M.; Galvagno, A.; Karlström, O.; Brink, A. Energy conversion of agricultural biomass char: Steam gasification kinetics. *Energy* **2018**, *161*, 1055–1063. [CrossRef]
38. Özkara-Aydınoğlu, Ş. Thermodynamic equilibrium analysis of combined carbon dioxide reforming with steam reforming of methane to synthesis gas. *Int. J. Hydrogen Energy* **2010**, *35*, 12821–12828.

Disclaimer/Publisher's Note: The statements, opinions and data contained in all publications are solely those of the individual author(s) and contributor(s) and not of MDPI and/or the editor(s). MDPI and/or the editor(s) disclaim responsibility for any injury to people or property resulting from any ideas, methods, instructions or products referred to in the content.